Nanoscale

Dynamic Article Links ►

Cite this: DOI: 10.1039/c0xx00000x

www.rsc.org/xxxxxx

ARTICLE TYPE

## Electronic Supplementary Information (ESI)

# This is the title Highly Conductive Three-Dimensional $MnO_2$-Carbon Nanotube-Graphene-Ni Hybrid Foams as Binder-Free Supercapacitor Electrodes

**Guoyin Zhu,[a] Zhi He,[a] Jun Chen,[a] Jin Zhao,[a] Xiaomiao Feng,[a] Yanwen Ma,*[a] Quli Fan,[a] Lianhui Wang[a] and Wei Huang*[a,b]**

## 1. $MnO_2$ mass measurement

The mass loading of $MnO_2$ on $MnO_2$-CNT-graphene-Ni hybrid was measured by by energy dispersive spectroscopy (EDS) and inductively coupled plasma-atomic emission spectroscopy (ICP-AES). To detect whether Ni was reacted with $KMnO_4$ or not, firstly we analyzed the content of Ni and Mn elements in hybrid and the reaction solution by EDS. The solid hybrid composite was dissolved by $HCl/HNO_3$ (3/1 in volume) solution. The reaction and dissolved solution were dropped onto two $SiO_2/Si$ substrates. The EDS spectrum (Fig. S1a) for the hybrid clearly shows the Mn and Ni signals while that for the reaction solution (Fig. S1b) does not present Ni signal any more. The Cl signal appears due to the utilization of HCl solution. The component and element content for these two samples are listed in Table S1. The Ni content in the reaction solution is zero while that in the hybrid is 22.8 wt%, suggesting Ni does not reacted with $KMnO_4$ solution in this case. In ICP-AES measurements, the Ni concentration in the reaction solution is rather low (0.01 wt %), further suggesting that no or trace of Ni participate the reduction of $KMnO_4$. The content of Ni and Mn was measured to be 94.39% and 5.61% (carbon was removed by combustion during sample preparation), corresponding to 8 wt% $MnO_2$ loading in the hybrid.

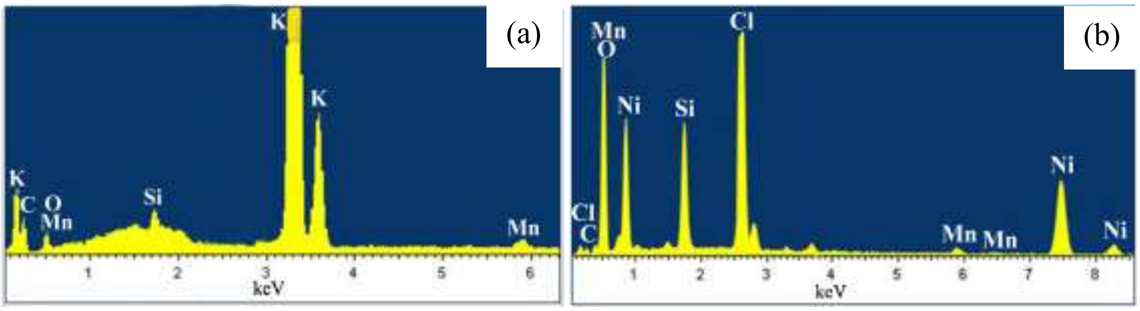

**Fig.S1** EDS of the reaction solution (a) and the $MnO_2$-CNT-graphene-Ni composite solution (b).

**Table S1** The elements content in the reaction solution and the $MnO_2$-CNT-graphene-Ni composites solution.

| samples | elements | | | | | | |
|---|---|---|---|---|---|---|---|
| | C | O | Si | Cl | K | Mn | Ni |
| **Reaction solution** | 5.91 | 13.47 | 1.02 | 0 | 77.92 | 1.67 | 0 |
| **Hybrid** | 7.04 | 43.22 | 6.75 | 19.19 | 0 | 0.95 | 22.84 |

## 2. The role of PEG in $MnO_2$ loading

In the synthesis of $MnO_2$, we used PEG as surfactant and reductant. The reaction of PEG could be roughly clued by measuring the Fourier transform infrared spectroscopy (FTIR) of the soluble byproducts remained in the solution. Fig. S2 shows the FTIR spectra of PEG before and after reaction. Obviously, some typical peaks from C=O in COOH appear after reaction, indicating the oxidation of PEG by $KMnO_4$. It is believed that $KMnO_4$ is apt to react with PEG rather than CNTs and the Ni foam coated by graphene because PEG has a plenty of active functional groups, such as C-H, C=C and C-OH. This will give much protection for carbon nanotubes and Ni skeleton. This result is given in ESI in the revised version.

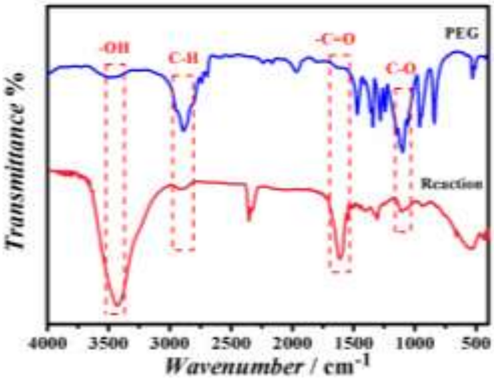

**Fig. S2** FTIR spectra of PEG before and after reaction.

## 3. The protection of Ni skeleton from electrolyte by graphene coating

It is true that in this work, there is no evident pseudocapacitance from the Ni foam because the electrolyte is isolated outside Ni by graphene coating.

Here CV and galvanostatic charge/discharge tests carried on three-electrode system—a more sensitive manner to measure the electrochemical reaction involved in electrode's surface than two-electrode system, were used to analyze the stability of Ni foam with and without graphene coating. As for the bare Ni foam (Fig. S3a), a pair of redox peaks at 0.5 and 0.58 V is observed, which can be assigned to $Ni^{2+}/Ni^{3+}$ redox couple formed on the Ni surface in the $Li_2SO_4$ electrolyte. When coated with graphene layer, however, the formed graphene-Ni foam does not give any redox peaks any more, even under tens of CV cycling (Fig. S3a). The disappearance of $Ni^{2+}/Ni^{3+}$ redox peaks on graphene-Ni foam suggests that there is no, or probably a negligible amount of electrolyte contacting with Ni foam. The corresponding galvanostatic charge/discharge tests also present the same result (Fig. S3b), i.e., the Faradaic process on bare Ni foam while the non-Faradaic precess on graphene-Ni foam. Hence it can be deduced that the Ni skeleton does not show its pseudocapacitance behavior and give little contribution to the total capacitance.

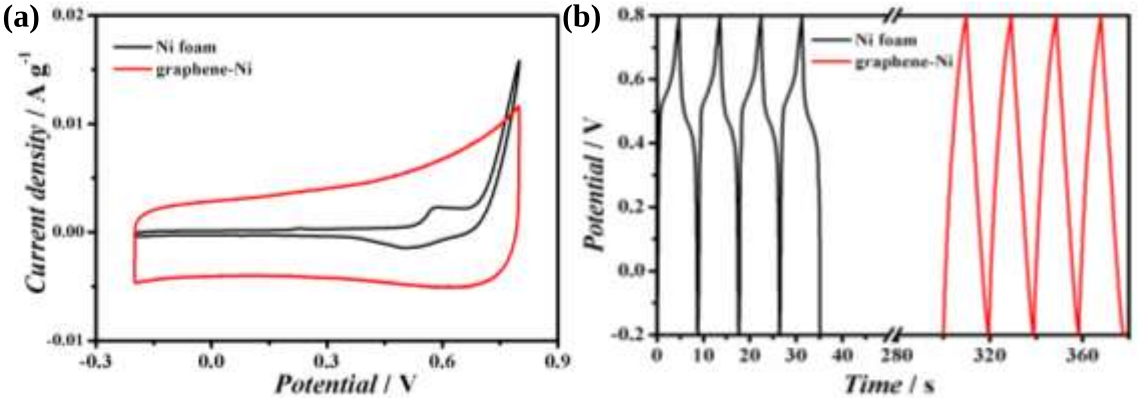

**Fig. S3** Stable CV curves at 100 mV/s (a) and galvanostatic charge/discharge curves within the potential window from -0.2 to 0.8 V (b) of Ni foam and graphene-Ni. The current densites in (a) are calculated using the total mass of the Ni and graphene-Ni electrode, which is different from the two-electrode test system.

## 4. The change of oxygen content on CNTs-graphene before and after $MnO_2$ loading

Since the oxidization of CNTs and graphene will give additional pseudocapacitance[1-4], the oxygen-containing functional groups existed on CNTs and/or graphene was analyzed by XPS. As shown in Fig. S4, the oxygen species on CNT-graphene-Ni is predominantly composed of C-O groups while those on $MnO_2$-CNT-graphene-Ni are the mixture of C-O, C=O and O=C-O groups due to the oxidation of $KMnO_4$. Their oxygen contents, however, do not give any difference as shown in Table S2. The C/O ratios before and after oxidation are 10.1 and 8.49, respectively. Therefore, it can be deduced that the oxygen-containing groups on CNTs are not the major factor that affects the capacitance. Moreover, in the calculation of the capacitance, the mass of CNTs and graphene were also incorporated into the total weight. Hence whether carbon was oxidized or not, their contribution to the capacitance is included.

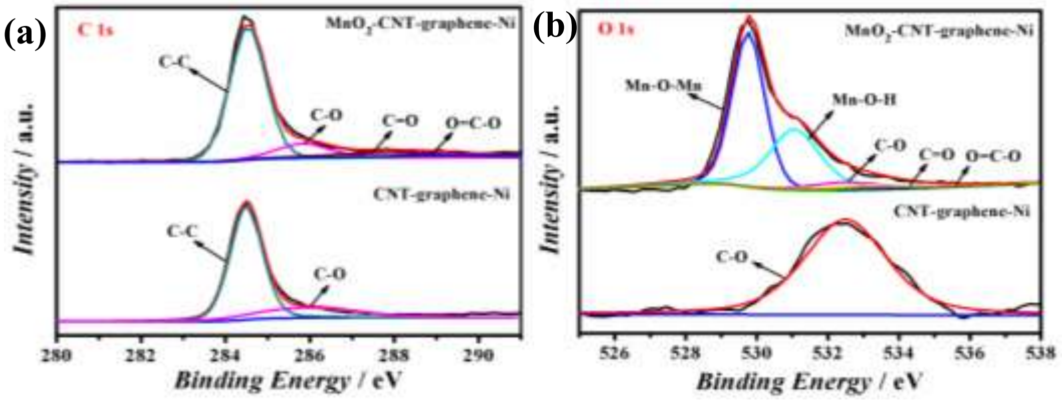

**Fig. S4** (a) C 1s XPS spectra and (b) O 1s XPS spectra of CNT-graphene-Ni and $MnO_2$-CNT-graphene-Ni.

**Table S2** Element content of C and O calculated from the C 1s XPS spectra in Fig. S4a.

| Samples | C/O ratio | Functional group | | |
|---|---|---|---|---|
| | | C-O(%) | C=O(%) | O=C-O(%) |
| CNT-graphene-Ni | 10.1 | 9.66 | 0 | 0 |
| $MnO_2$-CNT-graphene-Ni | 8.49 | 4.85 | 4.25 | 1.34 |

## 5. Galvanostatic charge/discharge curves of $MnO_2$-CNT-graphene-Ni electrodes

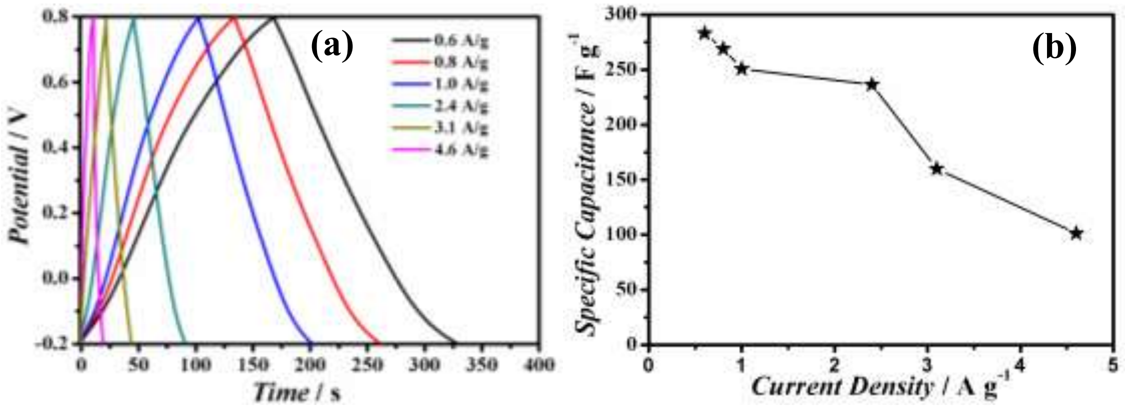

**Fig. S5** (a) Galvanostatic charge/discharge curves of $MnO_2$-CNT-graphene-Ni electrodes with voltage between -0.2V and 0.8 V at different current density; (b) The corresponding specific capacitance at different current density.

## 6. Equivalent circuit model

The equivalent circuit and the corresponding model are shown in Fig. S6. In the equivalent circuit (Fig. S6a), $R_E$ corresponds to combined resistance of intrinsic resistance of electrodes and the ionic resistance of electrolyte. $R_{CT}$ is charge transfer resistance. $C_{dl}$ represents the double-layer capacitance and $C_L$ is the limit capacitance.[5] $Z_W$ is Warburg resistance derived from the slope of the 45 ° portion of the curve, which is resulted from the frequency dependence of ion diffusion/transport in the electrolyte to the electrode surface.[6] As shown in Fig. S6b, the measured impedance curve is well consisted with the fitted one.

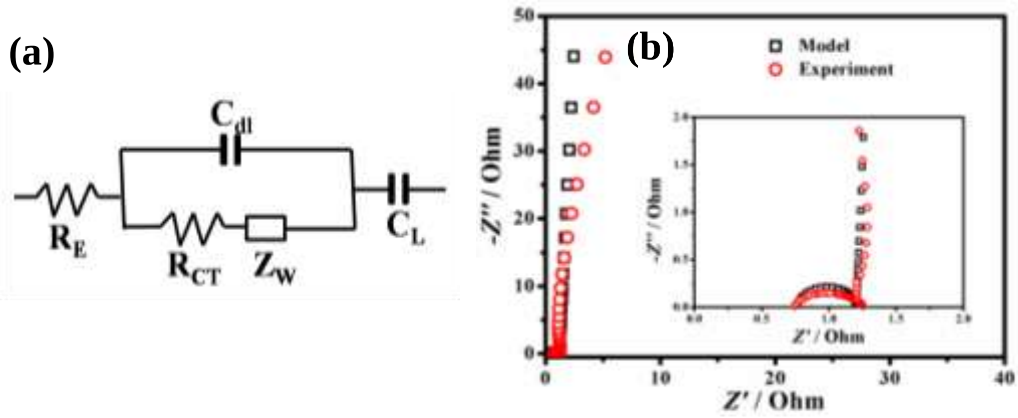

**Fig. S6**. (a) Equivalent circuit model of the device. (b) Measured and fitted Nyquist plots of the $MnO_2$-CNT-graphene-Ni electrodes.

## 7. The performance of reported $MnO_2$-carbon based supercapacitors

**Table S3.** Comparison of internal resistance ($R_s$) and specific capacitances ($C_s$) of the reported $MnO_2$/CNT, $MnO_2$/graphene and $MnO_2$/graphene/CNT composite-based electrodes

| Material Samples | $R_s$ (Ohm) | $C_s$ (F $g^{-1}$) | Scan rate/Current density | Test system | Ref# |
|---|---|---|---|---|---|
| **$MnO_2$/CNT composites** | | | | | |
| $MnO_x$/CNT/Ni | 2.8 | 462 | 5 A $g^{-1}$ | Three-electrode | 8 |
| $MnO_2$-CNT-sponge | 7 | 600 | 1 mV $s^{-1}$ | Three-electrode | 9 |
| $MnO_2$/CNT composite | 25 | 223 | 10 mV $s^{-1}$ | Three-electrode | 19 |
| $MnO_2$/CNT/PEDOT | 52 | 481 | 5 mV $s^{-1}$ | Three-electrode | 26 |
| $MnO_2$-CNT-textile | 20.4 | 410 | 5 mV $s^{-1}$ | Three-electrode | 28 |
| **$MnO_2$/graphene composites** | | | | | |
| graphene/$MnO_2$-textile | 48 | 315 | 2 mV $s^{-1}$ | Two-electrode | 10 |
| graphene/$MnO_2$ network | 7.8 | 130 | 2 mV $s^{-1}$ | Two-electrode | 13 |
| graphene-$MnO_2$ | 1.36 | 310 | 2 mV $s^{-1}$ | Three-electrode | 27 |
| graphene/$MnO_2$//ACN | 3.8 | 113.5 | 2 mV $s^{-1}$ | Two-electrode | 29 |
| AGMn | 0.34 | 850 | 0.25 A $g^{-1}$ | Two-electrode | 30 |
| **$MnO_2$/graphene/CNT composites** | | | | | |
| $MnO_2$ /graphene/CNT | 51 | 321 | 0.1 mA $cm^{-2}$ | Three-electrode | 6 |
| graphene/ $MnO_2$-CNT | 5 | 372 | 50 mV $s^{-1}$ | Three-electrode | 7 |
| CNT/$MnO_2$/GR | 15 | 486.6 | 5 mV $s^{-1}$ | Three-electrode | 31 |
| **Present work** | 1.25 | 251 | 1.0 A $g^{-1}$ | Two-electrode | |

## 8. Electrochemical performance of the all-solid-state supercapacitor

Fig S7a shows the all-solid-state supercapacitor lighted a light-emitting diode (LED) after charging. The specific capacitance calculated from the CV curve (Fig. S7b) at 10 mV $s^{-1}$ is 107 F $g^{-1}$, which decreases to 50 F $g^{-1}$ at 100 mV $s^{-1}$. Fig. S7c gives the charge/discharge curves at different galvanostatic current densities. These curves display a slight curvature, indicating the pseudocapacitive contribution along with the double layer contribution. As seen in the EIS (Fig. S7d), the solid supercapacitor owns an elevated internal resistance of 10 Ohm probably due to the high resistance of solid electrolyte.

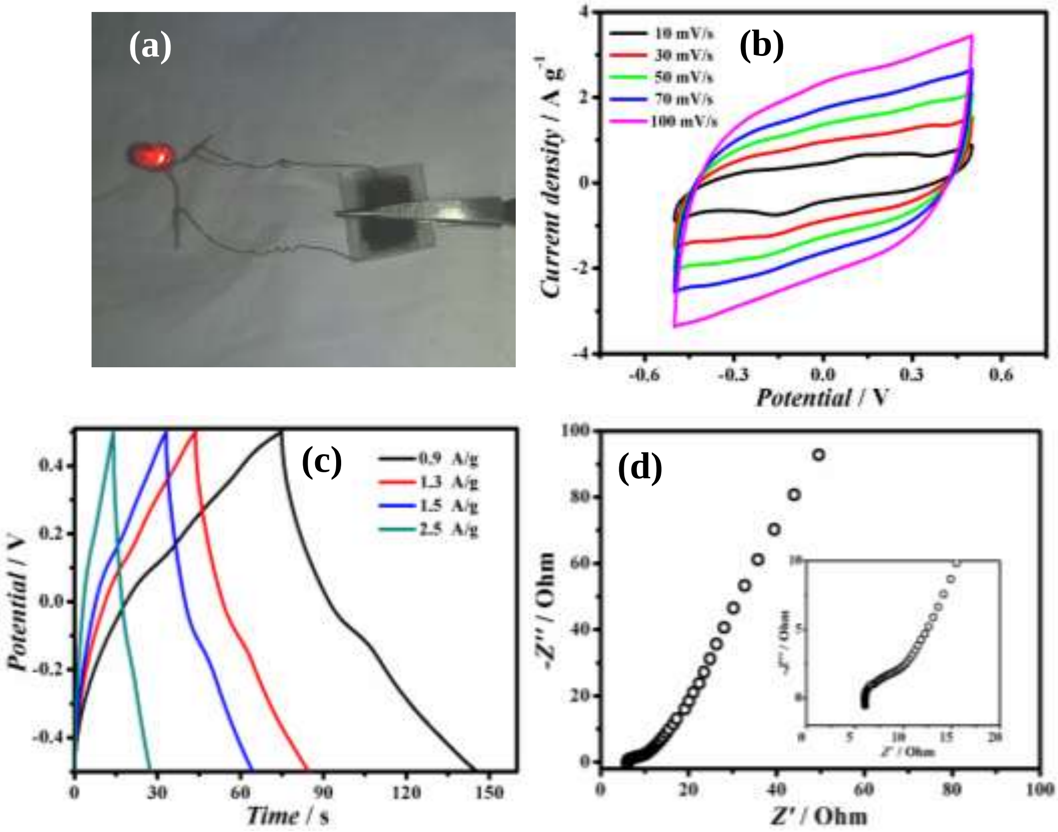

**Fig. S7.** (a)A digital photograph of a LED lighted by the supercapacitor, (b) Cyclic voltammograms, (c) the charge-discharge profile, and (c) Nyquist plots of the all-solid-state supercapacitor.

## References

1 L. X. Li, F. Li, *New Carbon Mater.* **2011**, 26, 224
2 S. W. Lee, B. M. Gallant, Y. Lee, N. Yoshida, D. Y. Kim, Y. Yamada, S. Noda, A. Yamada, Y. S. Horn, *Energy Environ. Sci.* **2012**, 5, 5437
3 C. T. Hsieh, W. Y. Chen, Y. S. Cheng, *Electrochim. Acta*, **2010**, 55, 5294.
4 L. Z. Fan, J. L. Liu, R. U. Din, X. Q. Yan, X. H. Qu, *Carbon* **2012**, 50, 3724.
5 M. S. Wu, C. Y. Huang, K. H. Lin, *J. Power Sources* **2009**, *186*, 557.
6 M. D. Stoller, S. Park, Y. W. Zhu, J. H. An, R. S. Ruoff, *Nano Lett* **2008**, *8*, 3498.